Numerical interpretation of regressive localized internal erosion in a real-scale levee physical model

Callari, Carlo; Pol, Johannes C.

DOI
10.1016/j.gete.2022.100395

Publication date
2022

Document Version
Final published version

Published in
Geomechanics for Energy and the Environment

Citation (APA)
Callari, C., & Pol, J. C. (2022). Numerical interpretation of regressive localized internal erosion in a real-scale levee physical model. *Geomechanics for Energy and the Environment*, *32*, Article 100395. https://doi.org/10.1016/j.gete.2022.100395

Important note
To cite this publication, please use the final published version (if applicable).
Please check the document version above.

Geomechanics for Energy and the Environment 32 (2022) 100395

Contents lists available at ScienceDirect

Geomechanics for Energy and the Environment

journal homepage: www.elsevier.com/locate/gete

Numerical interpretation of regressive localized internal erosion in a real-scale levee physical model

Carlo Callari [a,*], Johannes C. Pol [b]

[a] DiBT, Engineering Division, University of Molise, via De Sanctis 1, 86100 Campobasso, Italy
[b] Department of Hydraulic Engineering, Delft University of Technology, Stevinweg 1, 2628 CN Delft, Netherlands

ARTICLE INFO

Article history:
Received 10 July 2022
Received in revised form 2 August 2022
Accepted 20 August 2022
Available online 30 August 2022

Editors-in-Chief:
Professor Lyesse Laloui and Professor Tomasz Hueckel

Keywords:
Localized internal erosion
Backward erosion piping
Levees
Finite elements
Erosion kinetics
Multiphase porous medium

ABSTRACT

This paper presents the numerical interpretation of a recent experiment on a real-scale levee physical model, in order to investigate the process of Backward Erosion Piping (BEP) and validate a recently proposed finite element formulation able to model both the simultaneous processes observed in backward erosion piping, i.e. the propagation of the pipe tip and the enlargement of the conduit cross-section, as well as the time-dependent effects. In previous papers, the numerical formulation already demonstrated its ability in reproducing available experimental data of full-scale physical models of levees, e.g. for the IJkdijk and for the Delta Flume tests. In the present work, as a further validation for the aforementioned formulation, we consider the numerical interpretation of the regressive localized internal erosion observed in the newly constructed real-scale levee at the Flood Proof Holland facility test site in Delft, The Netherlands. This test was mainly focused on the experimental evaluation of the time-dependent effects typically observed in these phenomena. To this purpose the levee foundation was equipped with an effective and accurate pore water pressure monitoring system. The aforementioned formulation was considered for the numerical interpretation of the test, in view of its ability in modeling the time-dependent effects in backward erosion piping. Indeed, a good agreement between calculated and measured piezometric heads and pipe tip propagations was obtained.

1. Introduction

Internal erosion can lead to significant damage and catastrophic failure of hydraulic structures.[1–3] It covers a variety of erosion processes such as concentrated leak erosion, suffusion, contact erosion, and backward erosion.[4] Backward erosion can take two forms: backward erosion piping and global backward erosion. Backward erosion piping (BEP) is the internal erosion process by which groundwater flow under a structure erodes the granular foundation that is covered by a stable roof, forming a localized eroded zone, the so-called "erosion pipe".[5,6] As the erosion continues, this pipe progresses backwards, towards the water source. When a hydraulic shortcut is established between the downstream and the upstream sides of the hydraulic work, the pipe enlarges, rapidly leading to undermining of the structure.

Global backward erosion differs from BEP in that the soil is not able to hold a stable roof. This often results in larger voids, often progressing into the core of earth dams rather than in their foundation. This paper focuses on BEP, although the modeling approach may also be applicable to global backward erosion.

Assessment methods used in practice for the stability of structures against BEP are often empirical[1,7] or based on a strongly simplified representation of the processes.[8,9] See e.g. Ref. 10 for a short account of these engineering methods.

Numerical methods offer more flexibility in simulating complex geometries and soil variability. In contrast to the simplified approaches, some of these formulations also include the modeling of the erosion kinetics and are able to predict the time-dependent propagation of Backward Erosion Piping. Representative examples of these numerical methods have been presented in Ref. 11 which includes the application to full-scale physical models of levees and in Ref. 12 to small-scale physical models of cofferdams, described in Ref. 13. More recently, also a further extension of the formulation to hydro-mechanical coupling was proposed in Ref. 14 and applied therein to show the destabilizing effects of BEP on cofferdams.

Validation of numerical models of BEP requires experiments at different scales with detailed measurements of the erosion process. The BEP progression is due to the interaction of several processes: groundwater flow, pipe flow, enlargement of the pipe cross section, and pipe lengthening. The modeling of most of these sub-processes requires assumptions or calibration parameters. In particular the erosion laws have significant uncertainties and are empirical in nature.

* Corresponding author.
E-mail addresses: carlo.callari@unimol.it (C. Callari), J.C.Pol@tudelft.nl (J.C. Pol).

https://doi.org/10.1016/j.gete.2022.100395
2352-3808/

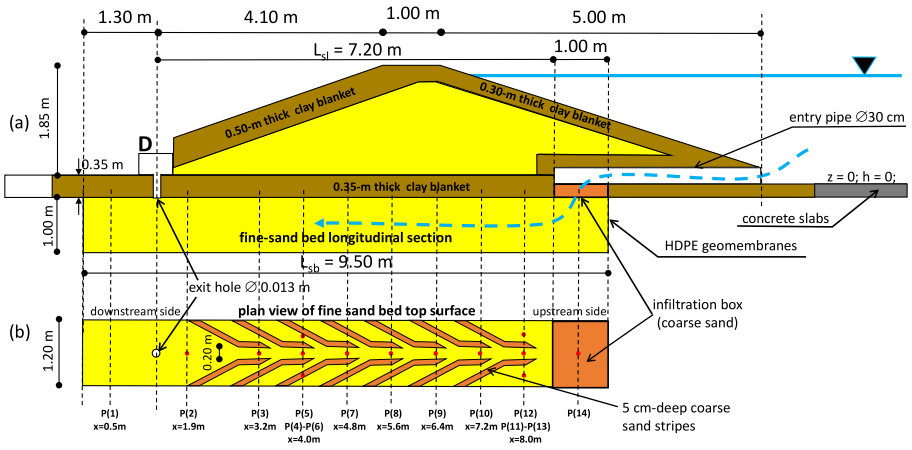

Fig. 1. Physical model of the real-scale levee recently constructed at the Flood Proof Holland test site: (a) dike cross section, including the fine-sand bed constructed below its foundation; (b) Plan view of the top surface of the fine-sand bed, with locations of 5-cm deep coarse sand stripes and of the n. 14 pore-pressure transducers installed just below the top surface.
Source: Modified from Ref. 18.

As a result, errors in one process can be compensated by errors in other processes. Therefore it is important to test such models on different experiments, both in terms of critical piezometric head, pipe progression and underlying processes. Especially large-scale BEP experiments are scarce in the literature. Two examples are the Delta Flume tests[15] and the IJkdijk tests[16] experiments. The Delta Flume tests are less suitable to validate erosion kinetics, because the experiments were stopped shortly after the critical piezometric head was reached. The IJkdijk experiments cover the full erosion process until failure. However, pipe development was derived from the pore pressure response which led to different interpretations,[17] possible because multiple pipes developed simultaneously.

Recently, a new BEP experiment was performed at Flood Proof Holland (FPH) facility in The Netherlands, in which pipe development in a earthen levee was closely monitored with pressure sensors.[18] The main objective of the present paper is to employ the results of this experimental test to validate the numerical model proposed in Ref. 11.

Hence, in the remainder of this paper, first the experimental setup and its results are briefly summarized in Section 2. Then, the main features of the employed numerical method are presented in Section 3. Finally, in Section 4, the numerical simulations of the test are presented and compared to the measured pipe progression in terms of pipe tip and piezometric head evolution, in order to assess the performance of the finite element formulation in reproducing the experiment at hand.

2. Experimental set-up and monitored response

A response simulated with the numerical method described in the next section is compared to the monitoring data obtained from a real-scale BEP experiment, aimed at measuring pipe progression rates (see Ref. 18 for a detailed description). The experiment was performed on a newly constructed levee at the Flood Proof Holland facility test site in Delft, The Netherlands.

As depicted in Fig. 1, below the levee foundation, a 9.5-m long, 1.0-m deep and 1.2-m wide fine-sand aquifer was constructed by excavating a trench in the clay and peat soil, perpendicular to the levee crest axis. Its sides and bottom were confined by a HDPE geomembrane, and the top of the aquifer was covered by a 0.35-m thick clay layer to obtain a realistic representation of the aquifer-blanket interface in the field. As illustrated in Fig. 1a,b, the flow enters the aquifer through a coarse-sand infiltration box installed on the top of the fine-sand bed and exits through a downstream-located 13-mm diameter exit hole which crosses the blanket. The seepage length $L_{sl} = 7.2$ m was obtained as the minimum distance between the infiltration box and the exit hole. The main aquifer fill consists of a compacted fine uniform sand ($d_{50} = 0.185$ mm, $d_{60}/d_{10} = 1.6$).

Small diagonal stripes of coarser sand ($d_{50} = 0.400$ mm) were included in the shallower 0.05 m of the sand bed (Fig. 1b) to allow for better measurements of pressures in the pipe, as explained below. The monitoring was primarily aimed at the measurement of pore pressures at the sand-clay interface (see Fig. 1b for the location of the n. 14 pore-pressure transducers installed just below the top surface of the fine-sand bed). The coarse-sand stripes were designed to prevent the pipe from growing sidewards and make sure that the pressures would have been measured within or close to the erosion pipe, which is crucial for an accurate monitoring of the pipe length development. Furthermore, the eroded sand mass was measured and the order of flow magnitude was obtained. Compared to other large-scale experiments at IJkdijk[6] and Delta Flume,[15] this close monitoring of the pressures is a major advantage.

Another important difference with previous large-scale experiments is the circular exit hole, compared to the otherwise totally unconfined aquifers at the downstream side. As a matter of fact, the circular exit hole results in the flow concentration which is typically found in the field. Unlike the Delta Flume experiments, the setup has a sand-clay interface instead of a perspex cover, and the experiment continued until the pipe had fully developed to the upstream side, which allows for a validation of the modeled temporal development after reaching the critical piezometric head.

The experimental procedure was to raise the upstream piezometric head step-wise, but only if the conditions had become stationary (no erosion). During the experiment, backward erosion piping developed through several phases: seepage without sand transport; fluidized sand filling the exit hole; sand boil formation; backward erosion reaching a stable state (the so-called "regressive phase"), and restarting of backward erosion (an unstable response, often denoted as "progressive phase"[8]) until the erosion front reaches the upstream water body. As the latter state was attained, the upstream piezometric head was decreased to stop the experiment.

The so-obtained critical piezometric head difference $H_c = 1.52$ m, after which erosion propagation was unstable, included approximately 0.10 m of piezometric head loss in the vertical

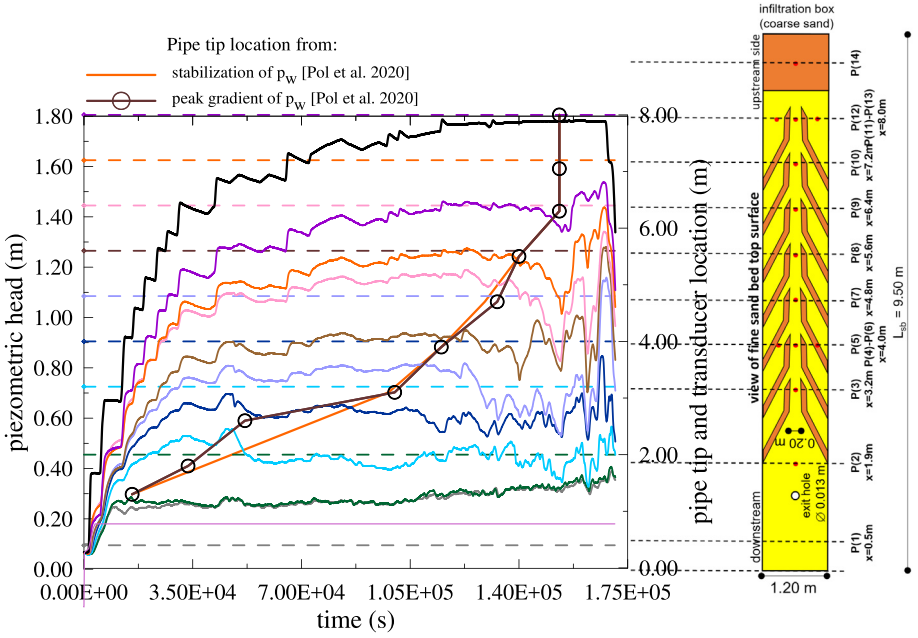

Fig. 2. Evolution of the piezometric heads measured during the FPH test, with location of the piezometric transducers on the top of the fine-sand bed. Also the two possible pipe tip propagation paths proposed in Ref. 18 are plotted.

exit hole. The corresponding critical pipe length was estimated as $l_c = 1.65$ m and the flow rate was approximately $2 \cdot 10^{-5}$ m^3 s^{-1}.

The evaluation of the pipe length progression was based on the principle that the passing of the pipe tip close to a transducer results in a peak in the local hydraulic gradient between such transducer and the next one in the upstream direction. Based on this assumption, the average progression rate for $l > l_c$ was $9 \cdot 10^{-5}$ m/s. When the pipe reached the upstream infiltration box, the eroded sand mass was approximately 10 kg, which increased further up to 17.5 kg at the end of the test due to pipe enlargement.

The piezometric head values measured along the central row of transducers are included in Fig. 2 using line plots without markers. Initially, the response follows the stepwise increase of the upstream piezometric head. At a later stage, the pressure gradually drops due to the draining pipe, in sequence from downstream to upstream transducers. This gradual pressure drop is followed by pressure fluctuations until the test ends, presumably caused by temporary clogging or meandering of the pipe.

3. Main features of the employed numerical method

The computational method proposed in Ref. 11 is employed to simulate the FPH test in the section that follows. This formulation is able to effectively model both the simultaneous processes observed in backward erosion piping, namely the propagation of the pipe tip and the enlargement of the conduit cross-section.

The numerical method is based on a novel formulation of the problem of localized erosion along a line propagating in a multidimensional porous medium. In this line, a conduit with enlarging transverse size is embedded, which conveys a multiphase flow. The two systems, porous medium and pipe, are bridged by exchange terms of multiphase fluid mass and by a shared field of fluid pressure.

Conversely, different fields are considered to describe flows, which are assumed as Darcian in the porous medium and turbulent in the conduit. These two flows drive pipe propagation and enlargement, respectively, as modeled by means of two proper erosion kinetic laws, recalled in the final part of this Section. The reader is referred to Sect. 2 of Ref. 11 for a fully detailed presentation of the "Governing Equations", including also the condition governing pipe propagation, which is based on the attainment of the critical porosity beyond the pipe tip. Among the several considered exchange terms, we mention the crucial source terms $m_w^{c,sw}$ and $m_w^{c,st}$ reported in balance eqns. (11) and (12) of Ref. 11, respectively, which account for the water mass gained by the conduit due to seepage through its wall and tip, respectively.

The corresponding numerical formulation assumes those frequent situations where the pipe location is a priori known with reasonable accuracy (as it is the case of the FPH test considered herein). Conforming combinations between one- and multidimensional finite elements are used to model the erosion conduit and the porous medium, respectively. We refer to Sect. 3 in Ref. 11 for a detailed presentation of the "Finite element formulation" including the mass balances at each node of the mesh and the procedure using the so-called "pipe-element candidates", introduced to simulate the tip propagation in discretized form. To this purpose, the current porosity in the pipe-element candidates is computed integrating the erosion kinetic law in the generic time step by a backward Euler scheme. Also the nodal balances and the so-obtained ordinary differential equations are written in residual algebraic form and integrated in the generic time step by a backward Euler scheme.

In Ref. 11, a fundamental role is played by the Appendix A "Finite element treatment of exchange terms", where it is shown that the two conduit source terms $m_w^{c,sw}$ and $m_w^{c,st}$ are both naturally taken into account in the aforementioned conforming combinations, together with the corresponding terms acting as localized sinks for the porous medium. This is a consequence of the conservative properties of the element nodal sources. Furthermore, as shown using arguments available in Refs. 19, 20, the element nodal sources provide a locally mass-conservative evaluation of outflows at finite element interfaces.

Several simulations were proposed in Ref. 11 to demonstrate the ability of the novel approach in reproducing available experimental data of full-scale physical models of levees, described in Ref. 16 for the IJkdijk test #2 and in Ref. 15 for the Delta Flume

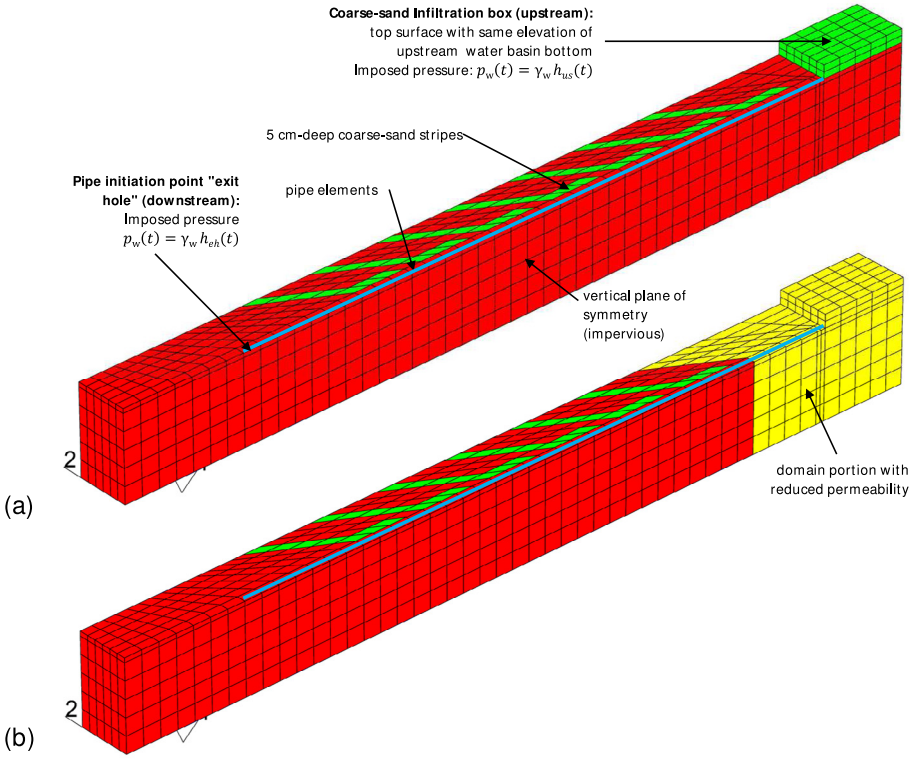

Fig. 3. Finite element discretizations considered for the sand bed domain (fine and coarse sand in red and green, respectively): (a) Finite element discretization of one half of the problem domain, in view of its symmetry with respect to the vertical and longitudinal mid-plane; (b) Finite element mesh including an upstream domain portion (in yellow) characterized by a lower (hydraulic) permeability, i.e. $k = 4.5 \cdot 10^{-5}$ m/s. (For interpretation of the references to color in this figure legend, the reader is referred to the web version of this article.)

tests T2, T3, T4. Our results point out the crucial role played by the combined influence of pipe propagation and enlargement, as well as of 3-D effects. We also assessed the mesh independence of the proposed numerical solution, particularly as concerns the calculated pipe propagation history.

In Ref. 11, the mass exchanged between the pipe and the porous medium due to erosion is expressed in the form of two prescriptions for the sink terms affecting the porous medium and relevant to the mechanisms of conduit enlargement and backward propagation, respectively. As concerns the tangential erosion mechanism, in both the aforementioned equations the mass gained by the conduit depends on the rate $\dot{A}$ of the pipe cross section area. Such a rate of conduit enlargement is computed herein in terms of pipe radius according to a typical law for tangential erosion[21–23]:

$$\dot{R} = \frac{c_t}{\rho_s}\langle \tau_t - \tau_{ct} \rangle \tag{1}$$

in which τ_t is the hydraulic shear stress at the erosion interface, c_t is the coefficient of tangential erosion and τ_{ct} is the critical value of shear stress for the activation of tangential erosion. In (1) the notation "$\langle\cdot\rangle$" denotes the positive part of "$\cdot$". Denoting by γ_w the water unit weight and by ξ the generic arc length distance from the pipe tip T, we compute the hydraulic shear stress using the expression:

$$\tau_t = \gamma_w \frac{R}{2}\left|\frac{\partial h}{\partial \xi}\right| \tag{2}$$

and estimate its threshold value according to the Shields criterion for the inception of sediment transport[24]:

$$\tau_{ct} = \theta\, d_s(\gamma_s - \gamma_w) \tag{3}$$

where the non-dimensional coefficient θ is the so-called Shields parameter, d_s is a characteristic particle diameter and γ_s is the solid-phase unit weight. With regard to the backward erosion mechanism ahead of the pipe tip, we assume that the exchange of the masses occurs at the instant when the following condition is satisfied:

$$n_T - n_{cr} = 0 \tag{4}$$

i.e. when the local porosity n_T attains the critical value n_{cr}. We note that the propagation condition (4) can otherwise be seen as a limit condition for the solid skeleton,[25] i.e. for the transition of a saturated porous medium into a fluidized soil–water mixture.[26] The numerical examples presented in Section 4 below show that the condition (4) effectively models the intermittent fluidization of sand in full-scale tests,[15,27] which was observed also in small- and medium-scale experiments.[6]

Prior to backward erosion, the increase of porosity n_T ahead of the pipe tip is computed as

$$\dot{n}_T = c_n\langle \tau_n - \tau_{cn} \rangle \tag{5}$$

where c_n is the coefficient of normal erosion, τ_n is a representative hydraulic shear stress and τ_{cn} is its critical value. The shear stress τ_n is computed at the pore network scale, i.e. at the wall of a "micro-conduit" whose diameter D_r is a representative pore diameter[28]:

$$\tau_n = \gamma_w \frac{D_r}{4}\,\|\nabla h\|_T\,, \qquad \text{with} \qquad D_r = 4\sqrt{\frac{2\,k_T\,\mu_w}{n_T}} \tag{6}$$

Namely, the representative shear stress τ_n is driven by the norm of the piezometric head gradient at the pipe tip $\|\nabla h\|_T$. The representative diameter D_r is estimated through the dynamic viscosity of water μ_w and the permeability at the tip k_T. The current value of k_T is computed as a function of n_T using the

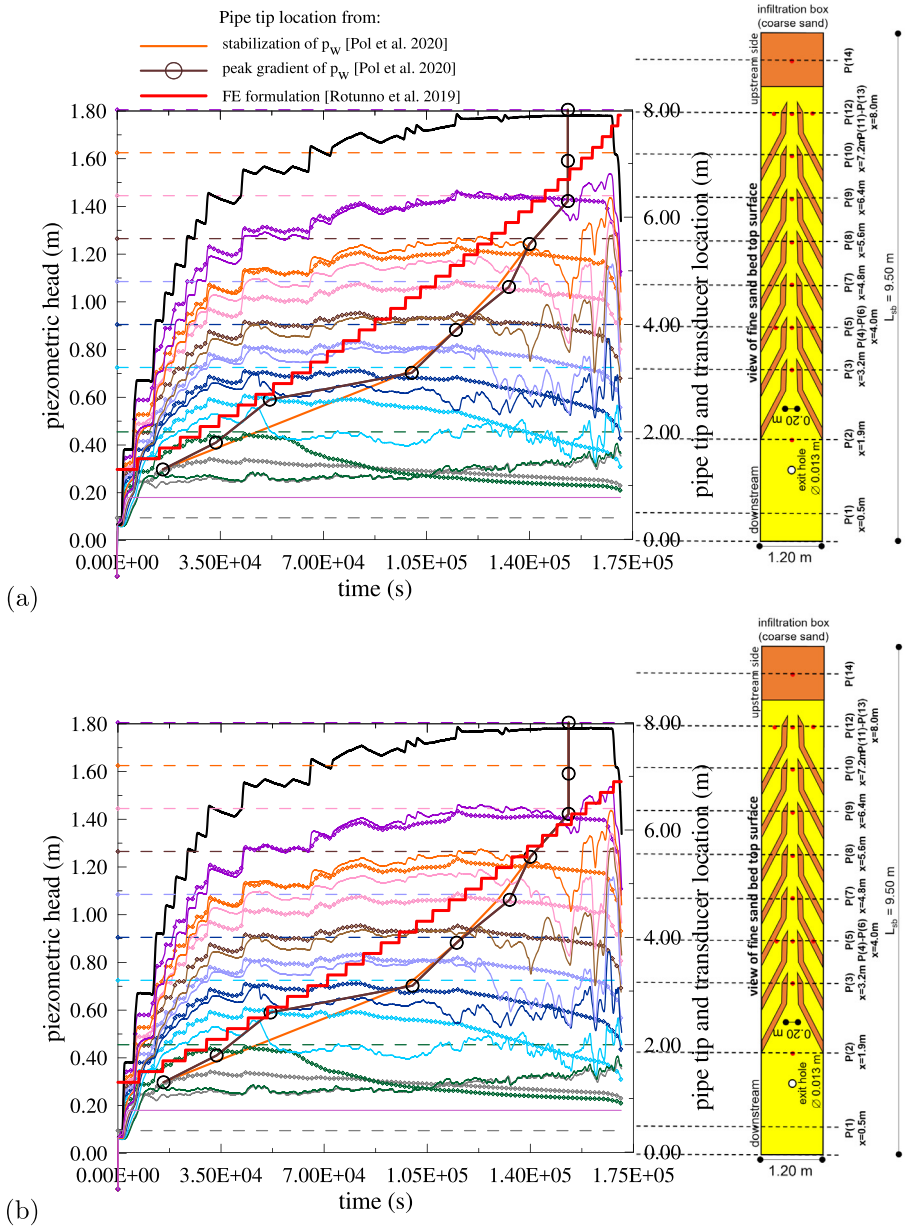

Fig. 4. Finite element simulation of the FPH test in terms of pipe tip propagation path, obtained from setting c_n = 1.30 kPa^{-1} s^{-1} (a) and c_n = 1.15 kPa^{-1} s^{-1} (b) and evolution of piezometric heads (calculated and measured curves are those with and without the markers, respectively). Both the graphs include also the two possible propagation paths obtained from experimental data in Ref. 18. The other employed parameters are those listed in bold in Table 1 for the FPH test. (For interpretation of the references to color in this figure legend, the reader is referred to the web version of this article.)

Kozeny–Carman relation[29]:

$$k_T = \left(\frac{n_T}{n_{T_0}}\right)^3 \left(\frac{1-n_{T_0}}{1-n_T}\right)^2 k_{T_0} \tag{7}$$

where n_{T_0} and k_{T_0} are the values of porosity and permeability at the pipe tip location prior to erosion. Though characteristic of a common approach to suffusion problems (e.g. Refs. 30–32), Eqs. (5)–(7) are assumed herein to cover also the situations in which the local increase of porosity is not driven by the erosion of the fine-grained fraction throughout a coarser matrix, but by the flow-induced damage or rearrangement of the whole granular skeleton (e.g. in poorly graded sand). In the latter scenario the same equations can be read as the reasonable statement that the degradation of the solid skeleton, ahead of the pipe tip, occurs at a rate that increases with the "excess drag" with respect to a threshold value.

The mass balances and the constitutive equations presented in Ref. 11 and briefly recalled herein can be contrasted with the approach by Wang et al. in Ref. 33, where a complete multi-phase formulation for localized erosion is missing and the crucial mechanism of pipe enlargement is not modeled.

4. Numerical simulation of the Flood Proof Holland test

As it can be inferred from Fig. 1b, the three-dimensional domain of the regressive localized piping erosion consists of the fine-sand bed, the coarse-sand stripes and the infiltration box. This domain is clearly symmetric with respect to its vertical and longitudinal mid-plane passing through the exit hole and the location of the pressure transducers from P(2) to P(14). Hence, in the numerical simulation of the test, we considered only one of the two domain halves separated by the mentioned symmetry

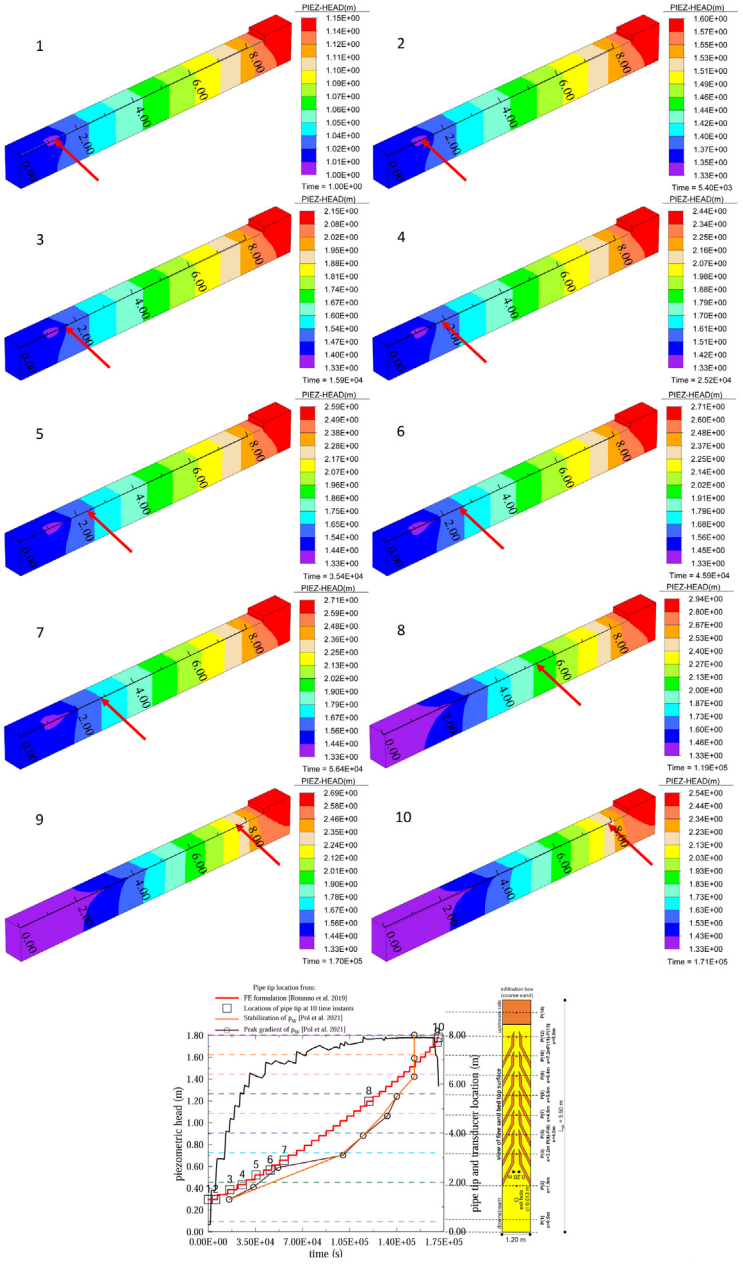

Fig. 5. FE results of the FPH test in terms of pipe tip locations (indicated by the arrow) in the mesh at 10 different time instants (marked in the graph), obtained for $c_n = 1.30$ kPa^{-1} s^{-1} The graph includes also the propagation paths obtained from experimental data by Ref. 18. The other employed parameters are listed in bold in Table 1 for the FPH test.

plane, as depicted in Fig. 3a. In this figure, some mesh details can be observed, namely the 5-cm coarse-sand stripes (in green) which have been generated in parametric form using code FEAP,[34] by imposing seven iterations of a 3-D periodic cell, which ensures conformity between the 1-D pipe elements and the 3-D solid elements, as well as a uniform distribution of the pipe-element lengths (0.20 m). The mesh is completed by the two 3-D blocks located upstream (including the coarse-sand infiltration box) and downstream (including the exit hole), respectively (consistently with Fig. 1).

In view of the experimental setting (see Section 2), where bottom and side boundaries of the sand bed were confined by a HDPE geomembrane and the top of the aquifer was covered by a 0.15-m thick clay layer, all the boundary surfaces where assumed as impervious, including the symmetry mid-plane.

On the contrary, as illustrated in Fig. 3a, boundary conditions on pore pressures are imposed at the top surface of the upstream infiltration box. This piezometric head was measured during the test for the rising water level in the basin. Also in the downstream area, the measured evolution of the piezometric head at the exit hole during the test was imposed, namely the initial condition of piezometric head $h = 0.065$ m at $t = 0$ s and the attainment, at $t = 3600$ s, of $h = 0.180$ m which was observed to remain practically constant up to the end of the test.

In view of the strong affinity between the sands employed for IJKdijk test #2, Delta Flume tests T2,T3,T4, and FPH, the erosion parameters employed herein for the FPH test (in bold in

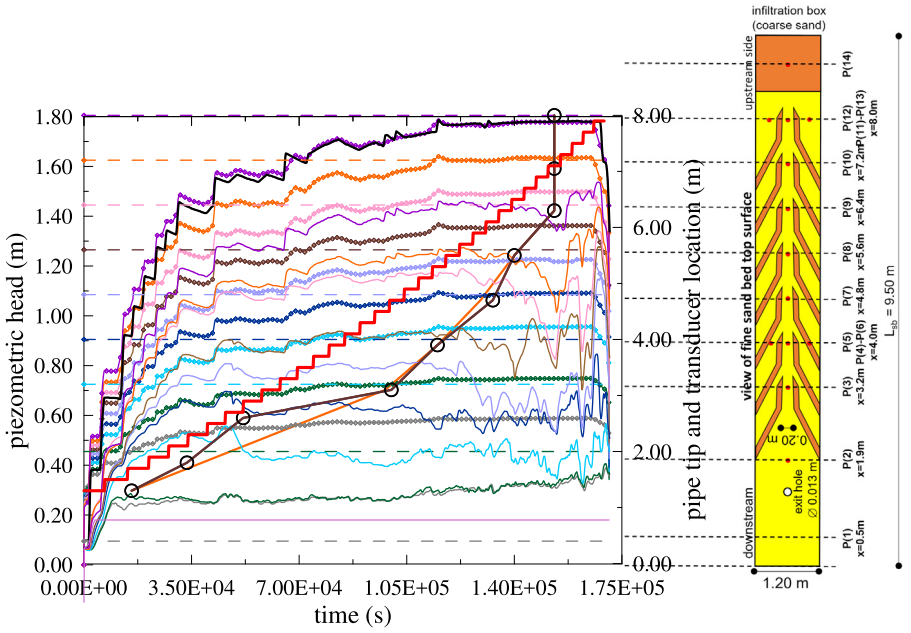

Fig. 6. FE simulation of the FPH test in terms of pipe tip propagation path, obtained from setting c_n = 1.15 kPa^{-1} s^{-1} and assuming *no permeability reduction due to clogging by fine sediments*. We note the differences between calculated and measured piezometric heads (curves with and without markers, respectively): the minimum and maximum values of such differences reach 0.28 and 0.55 m, respectively.

Table 1) were set as similar, but not necessarily coincident, to those already calibrated in Ref. 11.

In the preliminary computations, we observed that the measured piezometric heads, mainly by the upstream located transducers (P10, P12, P14) were always too much higher than the computed ones, as shown in Fig. 6. We conjectured that such differences were caused by an anomaly in the experiment or in measurements. In particular we noted that at such upstream locations, the piezometric head values measured by transducers at given time instants, e.g. those corresponding to the pipe tip passing a given transducer location, led to a measured piezometric head difference between adjacent transducers (e.g. P12 and P14) which was close to 25 cm.

However, given the hydraulic gradient of 0.15 cm/m in the aquifer (see Fig. S4 in Ref. 18) and the longitudinal distance of 50 cm from P12 to the upstream coarse-sand box (with P14 located within such box, see Fig. 1b), we would have expected about a 7.5-cm piezometric head drop instead of the measured 25 cm. In the test, also earlier and later of the given time instant, the measured piezometric head drop between P12 and P14 seemed too large. Among the possible reasons for such measured response we considered the following:

1. The distance between P12 and the coarse sand was larger than 50 cm (about 150 cm). However this explanation would require the distance measurement to be wrong by a factor of 3, which appears as a strongly unlikelihood event.
2. There was a leak in the clay cover around P12 which allowed water to seep into the sandy levee core. Then, the flow rate upstream of the leak is higher than downstream of it, with increase of the hydraulic gradient.
3. There is a lower conductivity between P12 and the coarse-sand upstream box, for instance because of clogging due to fine sediments deposited on the water basin bottom and transported by the water flowing into the upstream infiltration box.

The same likelihood can be practically assumed for the conjectures at points 2 and 3 above. Furthermore, it would have been very difficult to infer from the measurements which of the two situations occurred. Therefore, we finally decided to focus on the conjecture at point 3, since its modeling required less assumptions (just a change of conductivity in a region between P12 and the coarse-sand upstream box). On the contrary, the modeling of the conjectures at points 1 and 2 would have required assumptions on the boundary conditions such as the flow rate from the leak mentioned at point 2.

We considered this as a good argument for our approach, and we planned a set of further simulations in order to firstly define the domain homogeneously affected by fine sediment clogging (in yellow in Fig. 3b) and then we evaluated the properly reduced value of the (hydraulic) permeability, i.e. $k = 4.5 \cdot 10^{-5}$ m/s. Hence, by the numerical modeling of such an additional flow resistance, we finally computed lower piezometric heads, with strong reduction of the aforementioned head differences. For example, the mesh in Fig. 3b has been used for both the simulations illustrated in Fig. 4, leading to a significantly improved agreement between measured and calculated piezometric heads with respect to the results obtained with the mesh in Fig. 3a.

Some selected parameters, listed below, were subjected to fine tuning procedures using the criteria outlined in the following:

- We obtained the aforementioned "reduced" permeability value $k = 4.5 \cdot 10^{-5}$ m/s from a tuning finalized to reduce the difference between the computed and the measured piezometric heads (see details in the present Section 4);
- The erosion coefficient c_n for normal erosion mechanism was tuned to improve the agreement with the propagation history proposed in Ref. 18 on the basis of pore pressure measurements.
- Also the erosion coefficient c_t for tangential erosion mechanism was tuned to improve the agreement between the evolutions of measured and computed piezometric heads.

We remark that, as a consequence of the strong coupling between the variations of the erosion coefficients c_n and c_t (see Ref. 11), the tuning procedures oulined above were not straightforward. Anyway, the results presented in Ref. 11 and in this

Table 1
Model parameters employed in the numerical simulations of the IJkdijk test #2 and of the Delta Flume tests T2, T3, T4[11] as well as of the Flood Proof Holland (FPH) test considered herein (we recall that a further permeability value, i.e. $k = 4.5 \cdot 10^{-5}$ m/s is used to characterize the yellow domain portion in Fig. 3b).

Parameter	Symbol	Units	Test simulations in[11]		FPH test simulation
			IJkdijk test #2	Delta Flume T2,T3,T4	
As input					
Solid density	ρ_s	Mg m^{-3}	2.50	2.58	**2.61**
Water density	ρ_w	Mg m^{-3}	1.0	1.0	**1.0**
Water dyn. viscosity	μ_w	kN s m^{-2}	$1.35 \cdot 10^{-6}$	$1.35 \cdot 10^{-6}$	$\mathbf{1.52 \cdot 10^{-6}}$
Initial porosity (fine sand)	$n_{fs,0}$	–	0.380	0.385	**0.383**
Critical porosity (fine sand)	$n_{fs,cr}$	–	0.450	0.450	**0.485**
Ini. hydr. permeability (fine sand)	$k_{fs,0}$	m s^{-1}	$1.4 \cdot 10^{-5}$	$5.2 \cdot 10^{-6}$	$\mathbf{7.89 \cdot 10^{-5}}$
Hydr. permeability (coarse sand)	k_{cs}	m s^{-1}			$\mathbf{2.70 \cdot 10^{-4}}$
Calibrated in[11]					
Erosion coeff. for norm. mech.	c_n	kPa^{-1} s^{-1}	0.65	1.30	**1.15**, **1.30**
Crit. shear stress for norm. mech.	τ_{cn}	kPa	$1.0 \cdot 10^{-6}$	$1.0 \cdot 10^{-6}$	$\mathbf{3.00 \cdot 10^{-6}}$
Eros. coeff. for tang. mech.	c_t	s m^{-1}	$1.9 \cdot 10^{-5}$	$2.5 \cdot 10^{-5}$	$\mathbf{7.43 \cdot 10^{-6}}$
Crit. shear stress for tang. mech.	τ_{ct}	kPa	$1.75 \cdot 10^{-4}$	$1.62 \cdot 10^{-4}$	$\mathbf{1.85 \cdot 10^{-4}}$
Init. pipe radius	R_0	m	10^{-3}	10^{-3}	$\mathbf{10^{-3}}$

section demonstrate the robustness of our finite element formulation, also with respect to the parameter setting.

Both the graphs in Fig. 4 were obtained assuming $h_{EH} = 0.18$ m for the piezometric head at the downstream exit hole (its evolution is given by the magenta line in the graphs). The graphs differ exclusively for the values considered for the erosion coefficient c_n adopted to characterize the normal erosion mechanism, i.e. c_n = 1.30 kPa^{-1}s^{-1} in Fig. 4a and c_n = 1.15 kPa^{-1}s^{-1} in Fig. 4b.

The calculated red line plots of the discretized propagation history of the pipe tip obtained for both the aforementioned values of c_n are in acceptable agreement with those obtained from measured piezometric heads.

As it can be easily observed by contrasting Figs. 4a and 4b, the differences obtained from the considered variations of the c_n coefficient are quite significant in terms of slope of the pipe tip propagation path, but they are definitely less apparent in terms of variations of the piezometric head values.

On the contrary, in Fig. 6 obtained under the *assumption of no permeability reduction*, significant differences between calculated and measured piezometric heads are apparent. These results can be contrasted with the plots in Fig. 4, obtained assuming the aforementioned permeability reduction as a consequence of clogging due to fine sediments deposited on the water basin bottom.

As it regards the transducers from P5 to P12 (i.e. the upstream located transducers), both the graphs of Fig. 4 show indeed a very good agreement between calculated (line plots with markers) and measured (line plots without markers) piezometric heads, with the unique exception of the piezometric head measured by P9 (the pink measured line plot). As stated in Ref. 18 this might be explained by noting that the measured piezometric head at P9 is not consistent with the other locations. The transducers' spacing is 0.80 m from P3 to P12, so the head difference between those sensors should be similar. On the contrary, the head of P9 is about 0.05–0.10 m too close to P10 during the progressive phase.

A global view of all the measured and calculated heads in Fig. 4 confirms the conjecture about a possible inaccurate location or piezometric head measurement of the P9 transducer. As a matter of fact, the calculated location of the P9 piezometric head plot is definitely more consistent than the measured location of the P9 line plot (too close to P10).

In Fig. 5 the contour plots of piezometric heads in the mesh are reported for 10 different time instants, with the advancing pipe tip locations indicated by an arrow.

5. Conclusions

Among the main common causes of failure of hydraulic works, the hidden phenomenon of internal erosion is one of the most dreadful hazards for levees, dykes, and embankment dams. In the last decades, this hazard has been progressively increased as a consequence of the climate change, where the main threats are the increased water levels due to increased floods and sea level rise.

Accordingly, an increasing attention has been drawn to the development of new erosion tests and to early warning monitoring systems. Another important contribution of the research to the mitigation of internal erosion should be the formulation of advanced predictive numerical methods able to assess the erosion vulnerability of hydraulic structures, such as levees.

To this purpose, the objective of the present paper was a further validation of the finite element method proposed by Ref. 11 for the modeling of backward erosion piping. We used this formulation for the numerical interpretation of regressive localized internal erosion observed in the newly constructed real-scale levee at the Flood Proof Holland facility test site in Delft, The Netherlands.[18] This test was mainly focused on the experimental evaluation of the time-dependent effects typically observed in these phenomena. To this purpose the levee foundation was equipped with an accurate water pressure monitoring system.

In view of its ability in modeling the time-dependent effects in backward erosion piping, the formulation[11] was considered for the numerical interpretation of the test. A very good agreement was obtained between most part of calculated and measured upstream piezometric heads and pipe tip propagation histories.

On the contrary, as it regards the downstream transducers (from P1 to P3) the obtained agreement between calculated and measured piezometric heads was just fair. In next works, we plan to further investigate the reasons for this less satisfying results.

We also plan to further extend the formulation,[11] implementing the effects of localized piezometric head losses (e.g. at the exit holes) and test new erosion kinetic laws obtained from the results of numerical micromechanics studies employing DEM-LBM coupling[35]

CRediT authorship contribution statement

Carlo Callari: Conception and design of study, Acquisition of data, Analysis and/or interpretation of data, Writing – original

draft, Writing – review & editing. **Johannes C. Pol:** Conception and design of study, Acquisition of data, Analysis and/or interpretation of data, Writing – original draft, Writing – review & editing.

Declaration of competing interest

The authors declare that they have no known competing financial interests or personal relationships that could have appeared to influence the work reported in this paper.

Acknowledgments

The first Author was supported by a DiBT project on "Computational modeling of erosion". The research also benefited from several invitations of C. Callari at École Centrale de Lyon-LTDS. Suggestions were also kindly provided by colleagues during the meetings of the international research group GdRi-GeoMech of CNRS. The second Author was supported by the Perspectief research programme All-Risk with Project No. P15-21D, which is (partly) financed by NWO. Domain Applied and Engineering Sciences. Marta Cerri is acknowledged for the preliminary setting of the computations presented in this paper, during the preparation of her M.Sc. thesis at University of Rome "Tor Vergata".

All authors approved the version of the manuscript to be published.

References

1. Bligh W. Dams, barrages and weirs on porous foundations. *Eng News*. 1910;64(26):708–710.
2. Foster M, Spannagle M, Fell R. *Analysis of Embankment Dam Incidents*. University of New South Wales, School of Civil Engineering; 1998.
3. Fell R, Fry JJ. *Internal Erosion of Dams and their Foundations: Selected Papers from the Workshop on Internal Erosion and Piping of Dams and their Foundations, Aussois, France, 25-27 April 2005*. Taylor & Francis Group; 2007.
4. ICOLD. *Bulletin 164: Internal Erosion of Existing Dams, Levees and Dikes, and their Foundations*. ICOLD; 2017.
5. Hanses U, Müller-Kirchenbauer H, Savidis S. Zur Mechanik der rückschreitenden Erosion unter Deichen und Dämmen. *Bautechnik*. 1985;5:163–168.
6. Van Beek VM. *Backward Erosion Piping, Initiation and Progression* [Ph.D. thesis]. TU Delft; 2015.
7. Lane E. Security from under-seepage-masonry dams on earth foundations. *Trans Am Soc Civ Eng*. 1935;100(1):1235–1272.
8. Sellmeijer J, Koenders M. A mathematical model for piping. *Appl Math Model*. 1991;15(11):646–651. http://dx.doi.org/10.1016/S0307-904X(09)81011-1.
9. Schmertmann J. The no-filter factor of safety against piping through sands. In: Silva F, Kavazanjian E, eds. *Judgment and Innovation: The Heritage and Future of the Geotechnical Engineering Profession*. Reston: ASCE; 2000:65–132. In: Geotechnical Special Publication; http://dx.doi.org/10.1061/9780784405376.006.
10. Rotunno AF, Callari C, Froiio F. Computational modeling of backward erosion piping. In: *Models, Simulation, and Experimental Issues in Structural Mechanics*. Springer; 2017:225–234.
11. Rotunno AF, Callari C, Froiio F. A finite element method for localized erosion in porous media with applications to backward piping in levees. *Int J Numer Anal Methods Geomech*. 2019;43(1):293–316. http://dx.doi.org/10.1002/nag.2864.
12. Rotunno AF, Callari C, Froiio F. A numerical approach for the analysis of piping erosion in hydraulic works. In: *Lecture Notes in Civil Engineering: 26th Annual Meeting of European Working Group on Internal Erosion*. Springer; 2018:159–167.
13. Marsland A. Model experiments to study the influence of seepage on the stability of a sheeted excavation in sand. *Géotechnique*. 1953;3(6):223–241. http://dx.doi.org/10.1680/geot.1953.3.6.223.
14. Callari C, Froiio F. A hydromechanical finite element formulation for localized internal erosion in porous media, with application to backward piping in cofferdams. *Int J Multiscale Comput Eng*. 2020;18(2):181–197.
15. De Rijke WG. *Verificatie Piping Model: Proven in De Deltagoot*. Grondmechanica Report co-317710/7 (in Dutch); Delft; 1991.
16. De Bruijn H, Van Beek VM, Knoeff H, Koelewijn A. *Analyserapport IJkdijk pipingproeven*. Flood control 2015 project; Deltares; 2009.
17. Sellmeijer H, De la Cruz J, Van Beek VM, Knoeff H. Fine-tuning of the backward erosion piping model through small-scale, medium-scale and IJkdijk experiments. *Eur J Environ Civ Eng*. 2011;15:1139–1154. http://dx.doi.org/10.1080/19648189.2011.9714845.
18. Pol J, Kanning W, Jonkman S. Temporal development of backward erosion piping in a large-scale experiment. *J Geotech Geoenviron Eng*. 2021;147(2):04020168–1, 04020168–11. http://dx.doi.org/10.1061/(ASCE)GT.1943-5606.0002415.
19. Hughes T, Engel G, Mazzei L, Larson M. The continuous Galerkin method is locally conservative. *J Comput Phys*. 2000;163(2):467–488.
20. Diersch H. *FEFLOW: Finite Element Modeling of Flow, Mass and Heat Transport in Porous and Fractured Media*. Springer Science & Business Media; 2013.
21. Wan C, Fell R. Investigation of rate of erosion of soils in embankment dams. *J Geotech Geoenviron Eng*. 2004;130:373–380. http://dx.doi.org/10.1061/(ASCE)1090-0241(2004)130:4(373),
22. Wan C, Fell R. Laboratory tests on the rate of piping erosion of soils in embankment dams. *Geotech Test J*. 2004;27:295–303.
23. Bonelli S, Brivois O. The scaling law in the hole erosion test with a constant pressure drop. *Int J Numer Anal Methods Geomech*. 2008;32:1573–1595. http://dx.doi.org/10.1002/nag.683.
24. Chanson H. *The Hydraulics of Open Channels Flows: An Introduction*. 1st ed. Butterworth-Heinemann: Oxford, U.K.; 1999.
25. Yin H, Nur A, Mavko G. Critical porosity - A physical boundary in poroelasticity. In: *Int J Rock Mech Min Sci Geomech Abstr*. Pergamon; 1993:805–808. 30.
26. Cubrinovski M, Ishihara K. Maximum and minimum void ratio characteristics of sands. *Soils Found*. 2002;42(6):65–78.
27. Van Beek VM, De Bruijn H, Knoeff J, Bezuijen A, Forster U. Levee failure due to piping: a full-scale experiment. In: *Scour and Erosion. Proceedings of the Fifth International Conference on Scour and Erosion (ICSE-5), San Francisco, California, USA, 7-10 November, 2010*. 2011:283–292.
28. Ojha C, Singh V, Adrian D. Determination of critical head in soil piping. *J Hydraul Eng*. 2003;129(7):511–518.
29. Carman P. Flow of gases through porous media, 1st ed. Butterworths; 1956.
30. Zhang X, Wong H, Leo C, Bui T. A thermodynamics-based model on the internal erosion of earth structures. *Geotech Geol Eng*. 2013;31:479–492. http://dx.doi.org/10.1007/s10706-012-9600-8.
31. Albertson M, Barton J, Simons D. *Fluid Mechanics for Engineers*. Prentice-Hall; 1968.
32. Fujisawa K, Murakami A, Nishimura S. Numerical analysis of the erosion and the transport of fine particles within soils leading to the piping phenomenon. *Soils Found*. 2010;50(4):471–482.
33. Wang D, Fu X, Jie Y, Dong W, Hu D. Simulation of pipe progression in a levee foundation with coupled seepage and pipe flow domains. *Soils Found*. 2014;54(5):974–984.
34. Taylor RL. *FEAP - A Finite Element Analysis Program: Version 8.2 Theory Manual*. University of California at Berkley; 2008.
35. Froiio F, Callari C, Rotunno A. A numerical experiment of backward erosion piping: kinematics and micromechanics. *Meccanica*. 2019;54:2099–2117. http://dx.doi.org/10.1007/s11012-019-01071-7.